Characterization of Mg-rich natural serpentine clay mineral and removal of reactive blue 19 from aqueous solutions

Gökçe Didar Değermenci[1]*, Nejdet Değermenci[1], Nuray Emin[2], Elif Aşıkuzun[3]

1 Department of Environmental Engineering, Kastamonu University, Kastamonu, Turkey
2 Department of Biomedical Engineering, Kastamonu University, Kastamonu, Turkey
3 Department of Metallurgical and Materials Engineering, Kastamonu University, Kastamonu, Turkey

*Corresponding author E.mail: gdegermenci@kastamonu.edu.tr

Abstract
The present study assessed the use of serpentine clay as adsorbent to remove the anionic dye agent of Reactive Blue 19 (RB19) from aqueous solutions. Firstly, serpentine clay minerals were characterized using different instrumental techniques like XRD, FTIR, SEM, TGA, XRF and BET analysis. As a result of characterization, the clay sample was determined to be serpentine group and it contained antigorite as dominant mineral type. Later, adsorption studies were performed and the effects of initial pH, adsorbent dosage, initial dye concentration and temperature on RB19 removal were investigated. The experimental results determined the highest adsorption capacity was obtained as 44.8 mg/g with initial RB19 concentration of 200 mg/L, temperature 25°C, adsorbent concentration 2 g/L and pH 7. According to isotherm results, the Langmuir isotherm model was more suitable to explain adsorption of RB19 on serpentine compared to the Freundlich isotherm model. Additionally, adsorption data indicate the pseudo-second-order kinetic model is a better fit rather than the pseudo-first-order kinetic model.

Introduction

To meet the increasing demand for clean water on a global scale, it has become common to treat wastewater to make it reusable. Currently, more than 7000 dyes and pigments with different chemical structures are commonly used in many industries like cosmetic, textile, paper, pharmaceutical, food and leather industries (Nidheesh et al., 2018). Among these sectors, the textile industry comprises the largest portion with mean water use of 40 m³/ton. Traditional treatment facilities can only treat 20-30% of the synthetic dyes sourced in the textile industry and dye concentrations may reach 200 mg/L in textile industry discharge water (Melo et al., 2018; Nga et al., 2020). As color names of colorants based on chemical structures are complicated, common names are frequently used, with synthetic dyes generally classified as acid, basic, direct, dispersed and reactive dyes (Tkaczyk et al., 2020). Reactive dyes are generally classified as azo and anthraquinonoid dyes linked to the

complex aromatic molecular structures (Arshad et al., 2020). Reactive dyes enter reactions with functional groups on fibers forming covalent bonds and are anthraquinone dyes chosen due to high dye fastness. Anthraquinone dyes are more toxic, resistant organo-pollutants for human cells in addition to bacteria compared to azo dyes and so are more difficult to treat with traditional methods (Chaudhari et al., 2017). In the literature, many methods have been applied for removal of Reactive Blue 19 including the Fenton oxidation process (Değermenci and Akyol, 2020), electrochemical oxidation (Vasconcelos et al., 2016), photocatalytic (Bilal et al., 2018), sono/photo/sonophotocatalytic (Khan et al., 2015), electrocoagulation/ coagulation (Taheri et al., 2013), sonoelectrocoagulation (He et al., 2016), and adsorption (Değermenci et al., 2019; Kocaman, 2020). Among these methods, the adsorption process is chosen due to convenient application and low cost. For the adsorption process, a variety of adsorbents like waste raw materials, active carbons and clay minerals are used. Clay is a raw material with a variety of properties and fields of use related to its mineral structure and components. Clay minerals are basically aluminum hydrosilicates with aluminum fully or partly replaced by Fe or Mg in some minerals. Serpentinite is an ultramafic rock containing high rates of Mg and Fe and mafic minerals like olivine. Serpentinite contains serpentine mineral groups like antigorite, chrysotile and lizardite, three polymorphs with the same chemical composition and different crystal structures (Lacinska et al., 2016). Serpentine is an octahedral layered silicate mineral with regular porous structure and strong surface activity with 1:1 layering and basic crystal structure $[Mg_3Si_2O_5(OH)_4]$ (Cao et al., 2017). Serpentine's acid-base properties in water are connected to the acidic silicate layers and basic brucite-like layers. As a result, it displays buffering features in acidic and alkaline solutions (Momčilović et al., 2016). Compared to other clay minerals, it is preferred due to the good adsorption of most chemical substances, the abundant amount of OH^- groups on the surface, carbon dioxide

capture and storage, potential source of nickel and as a raw material (metallic magnesium and/or pure magnesium compounds) properties (Shaban et al., 2018). Momčilović et al. (2016) studied significant potential to adsorb lead and dyes from synthetic waters (Momčilović et al., 2016). Shaban et al. (2018) conducted studies using it as an adsorbent material for methylene blue dye, congo red dye, and Cr(VI) ions and found that the effect of thermal and acid treatments has increased the adsorption capacity (Shaban et al., 2018). In their study, Cao et al. (2017, 2019) increased the adsorption capacity by thermal activity modifications for the adsorption of Pb^{2+} and Cd^{2+} using serpentine (Cao et al., 2019, 2017). Huang et al. (2017) investigated activated serpentine with secondary treatment for both copper recovery and treatment and lowered discharge limits (Huang et al., 2017). In this study, firstly clay obtained from the Çankırı-Korgun region was characterized. With the aim of determining the physical and chemical characterization of serpentine as adsorbent, XRF, XRD, TGA, FTIR, SEM and BET analyses were completed. The clay with serpentine crystal structure was investigated for efficacy for use as adsorbent for probable pollutants. In line with this aim, the serpentine clay was used as adsorbent to remove pollution caused by a reactive dye matter in industrial wastewater with the adsorption method. The effects of dye concentration, adsorbent dosage, temperature and pH parameters on adsorption were investigated. Experimental data obtained from the adsorption of dye on serpentine was analyzed with different adsorption isotherms and kinetic models.

Materials and Methods

Materials

The clay sample used in the experimental study was obtained from Korgun county in Çankırı province located in the Central Anatolian region of Turkey. The clay had no preliminary procedures applied. After clay for use in experiments was ground with the aid of appropriate crushers and grinders, it was sieved to 125-250 micrometer grain size with the

aid of molecular sieves to obtain clay minerals. Reactive Blue 19 (RB19) dye was obtained from a textile factory located in Bursa, Turkey. The properties and molecular structure (Taheri et al., 2013) of RB19 are shown in Table 1 and Figure 1, respectively (Isah et al., 2015). To set the necessary pH for dye solutions, 0.1 M H_2SO_4 and NaOH were used.

Table 1. *General properties and chemical structure of RB19.*

Generic name	Reactive Blue 19
Commercial name	Remazol Brilliant Blue R
Abbreviation	RB19
Functional group/Chemical base	Anthraquinone
CAS number	2580-78-1
C.I. number	61,200
λ_{max} (nm)	593
Molecular mass (g/mol)	626.54
Solubility	30 g/L in water @ 80°C
pH of stock solution	6.20 @ 28°C
Molecular formula	$C_{22}H_{16}N_2Na_2O_{11}S_3$
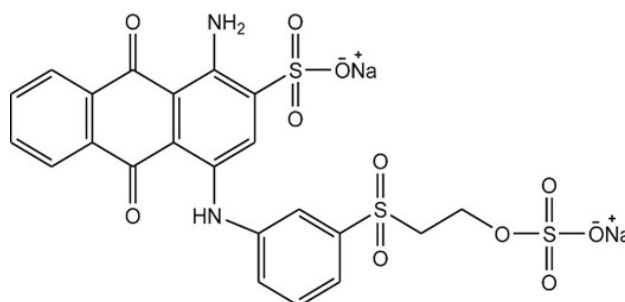
Figure 1. *Molecular structure of RB19.*

Adsorption experiments

Batch adsorption experiments were completed on a temperature-controlled stirrer (IKA KS 3000i) with fixed mixing rate (300 rpm) in 50 mL Erlenmeyer flasks. A stock solution (1000 mg/L) was prepared by dissolving the RB19 dye in distilled water. The adsorption of RB19 dye on unprocessed natural clay was investigated with optimum conditions determined based on the effects of initial solution pH from 3-9, different initial concentrations of 100-300 mg/L, adsorbent amounts 0.005-0.3 g/50 mL and temperature 25-55°C. During the study, Langmuir and Freundlich isotherms were calculated. RB19 concentration was measured with a UV spectrophotometer (Hach Lange DR6000) at the maximum wavelength for RB19 (λ=593 nm). Equilibrium adsorption capacity (q_e), adsorption capacity at time t (q_t) and dye removal efficiency (R) were obtained using Eq. [1], [2] and [3], respectively:

$$R(\%) = \left[(C_0 - C_e)/C_0 \right] \times 100 \quad [1]$$

$$q_e = \left[(C_0 - C_e)/m \right] \times V \quad [2]$$

$$q_t = \left[(C_0 - C_t)/m \right] \times V \quad [3]$$

where C_0 is the initial concentration of RB19 dye (mg/L), C_e is the equilibrium concentration of RB19 dye (mg/L), C_t is the concentration of RB19 dye (mg/L) at t time, V is the volume of RB19 dye solution (L), and m is the weight of serpentine (g).

Adsorbent characterization techniques

The dimension and morphology of the serpentine before adsorption was observed with a scanning electron microscopy (FEI model Quanta FEG250), operated at 15 kV. Clay samples were coated

with gold in a vacuum environment before SEM observation. The changes in vibrational frequencies of surface functional groups in the serpentine were analyzed using a Fourier Transform Infrared (ATR-FTIR, Alpha II, Bruker) spectrometer in the spectral range of 400-4000 cm^{-1} (resolution 4 cm^{-1}, scans 24). The specific surface area of the samples was estimated by Brunauer-Emmet and Teller model (BET) with the pore volume and size were measured using the Barrett-Joyner-Halenda (BJH) formula.

The chemical composition of serpentine was analyzed by using X-Ray Fluorescence Spectroscopy (Spectro brand Xepos II model). The detector on the instrument is a silicon drift detector, and the resolution remains stable, regardless of the count rate. Also, it has internal collimators that greatly improve the signal/noise ratio.

X-ray Diffraction measurements were carried out by Bruker D8 Advance X-ray powder diffractometer device using Cu K$_\alpha$ radiation source (λ=0,154 nm). Scanning rate used 2θ angle ranging from 3° to 90° incremented and scan speed 2°/min.

Thermal gravimetric analysis of serpentine was done by employing Thermo Gravimetry/Differential Thermal Analyzer (HITACHI STA7300 Model). Serpentine weighing 5.584 mg was placed into an alumina sample pan and heated from 25 to 1000°C at a heating rate of 20°C/min under a nitrogen atmosphere with flow rate of 20 mL/min.

Results and Discussion

Characterizations

Analyses were performed with the aim of determining the chemical composition and crystal structure of the clay sample. Attempts were made to identify the element composition with XRF and the molecular structure with FTIR. Thermal characteristics were determined using TG-DTA analyses, while attempts were made to explain crystal structure with XRD. Surface morphology was illustrated by investigation with SEM. Finally, the total surface area and mean pore size were determined for the material.

Elemental Composition. The chemical composition of the clay sample was characterized by XRF and results are given in Table 2. The majority of the clay sample comprised MgO and SiO$_2$. Other elements like Fe, Al, Na, Ca, Ni and Cr were observed in various compositions. In fact, the high silica and magnesium percentage in the sample proves the presence of serpentine. The serpentine group contains minerals relatively poor in terms of silica (<45% SiO$_2$) (Horen et al., 2014). Serpentine is rich in magnesium and was reported to have Mg/Si ratio of nearly 1.5 (Yalçin and Bozkaya, 2006). The studied clay sample had Mg/Si ratio of nearly 1.6. The general structure of the clay may be written as MgO:SiO$_2$:Fe$_2$O$_3$ and the mass composition of these compounds has ratio of 8:5:1 with molar composition of 18:9:1.

Table 2. *Composition of clay sample based on XRF (weight %).*

Component (%)	MgO	SiO$_2$	Fe$_2$O$_3$	Al$_2$O$_3$	Na$_2$O	CaO	NiO	Cr$_2$O$_3$
Concent (%)	53.35	41.76	5.94	0.52	0.49	0.33	0.22	0.16

Crystal Structure Analysis. According to the XRD model for the natural clay samples (Figure 2), the sample contains main clay mineral serpentine (Mg$_3$Si$_2$O$_5$(OH)$_4$) with submineral types of antigorite, lizardite and chrysotile (Emrullahoglu Abi et al., 2015; Teir et al., 2007).

Antigorite, lizardite and chrysotile display similar XRD patterns and have characteristic diffraction peaks in close locations. The characteristic sharp peaks for serpentine are at 2θ=12.18°, 24.26° and 34.41°. When XRD data of all samples are analyzed, the SiO$_2$, Fe$_2$O$_3$ and Mg peaks are found predominantly. SiO$_2$ reflection peaks are oriented along the (311) and (533) planes, at approximately 2θ=12.18° and 24.26° degrees, respectively.
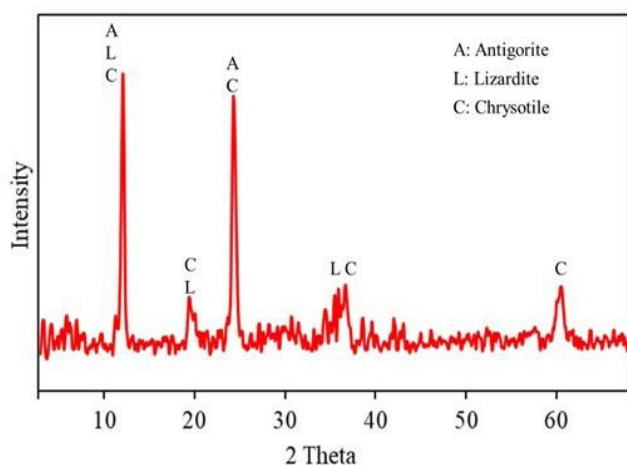
Figure 2. *XRD patterns of raw serpentine clay.*

Figure 3 . *TG and DTA curves of serpentine sample.*

And also, Mg reflection peaks are observed at 2θ=34.41° and 36.59° degrees represent the (002) and (101) planes, respectively and Fe_2O_3 peaks which are reflected from (130) and (144) planes are found at 2θ=35.86° and 60.27° degrees.

Grain size value was calculated via the X-Ray diffraction patterns, and it has great importance due to characteristics for engineering, industrial and technological applications of materials. Warren-Scherrer method is used for grain size value calculation (Patterson, 1939). For details see below (Eq. [4] and [5]):

$$D = 0.944 \frac{\lambda}{B \cos \theta} \qquad [4]$$

$$B^2 = B_s^2 - B_m^2 \qquad [5]$$

where, D denotes the grain size, λ presents the wavelength of the X-ray used and B depicts the full width half of the maximum peak intensity in the radian unit. Also, B_m is a constant value when θ is an angle belonging to this peak. The result of the average grain size calculations is 17.12 nm.

Thermal analysis. The phase changes and mass variations occurring in the sample linked to temperature increase were determined with TG-DTA analysis. According to the DTA curve, an endothermic peak was observed at 654°C with an exothermic peak observed at 834°C (Fig. 3).

Serpentine contains the three related minerals of antigorite, lizardite and chrysotile. Studies of serpentine minerals found a broad endothermic peak between 500 and 800°C and an exothermic peak showing formation of a new mineral between 800 and 850°C (Dlugogorski and Balucan, 2014; Gürtekin and Albayrak, 2006; Viti, 2010). The endothermic peak represents release of structural water from the mineral, while the exothermic peak represents formation of forsterite and enstatite as a result of destruction of the crystal structure of serpentine (Cheng et al., 2002). As a result, the endothermic peak at 654°C shows the release of structural water from the serpentine mineral and the exothermic peak at 834°C is an indicator of the formation of forsterite and enstatite. Mass loss was observed in three regions for the serpentine sample; at temperatures 200°C, from 350-450°C and >550°C. The mass loss observed from the serpentine sample from 500 to 800°C was 11.3%. TGA analysis of serpentine complies with results reported in the literature (Maroto-Valer et al., 2005; Viti, 2010; Viti et al., 2011).

Surface Area and Porosity. The specific surface area and average pore size of serpentine was determined by the Brunauer-Emmett-Teller technique that is an important analysis. Results obtained from the nitrogen adsorption-desorption isotherms of the clay sample are given in Table 3. Isotherms can be classified as type IV(a) according to the IUPAC

with an H3 type hysteresis loop (Thommes et al., 2015). The clay sample used in the study had 31.87 m²/g surface area. The high surface area of the natural clay sample is an indicator that it can be used as adsorbent. Type IV(a) isotherms are given by mesoporous adsorbents. The average pore radius of natural clay was found to be 2.18 nm.

Table 3. *Surface properties of serpentine.*

Parameters	Values
Multipoint BET surface area (m²/g)	31.87
BJH Adsorption cumulative volume of pores (cm³/g)	0.0066
BJH adsorption pore radius (nm)	2.18

Morphological Analysis. The micromorphology of the unprocessed natural serpentine clay was investigated by a scanning electron microscope. The serpentine group contains three polymorphs of chrysotile, lizardite and antigorite. A study stated that chrysotile is fibrous, lizardite is very fine-grained and flat, while antigorite forms grooved plates or fibers (Karunaratne, P. C. T., Fernando, 2015). Another study stated that antigorite and lizardite are dense or fine-grained, while chrysotile is a fibrous variety (Ballotin et al., 2020; Hršak et al., 2008). Serpentine group minerals were observed as parallel and layered aggregates with fibrous arrays of long rods on micrographs. These rods may be attributed to the presence of chrysotile and mean size was measured as 60 nm wide and 1 μm long. Before treatment of clay samples with dye, it appears there were free small extensions and fibrous structures expanding the surface area of the structure (Figure 4: A, C).

After treatment with RB19, there appeared to be a reduction in free structures on the surface (Figure 4:
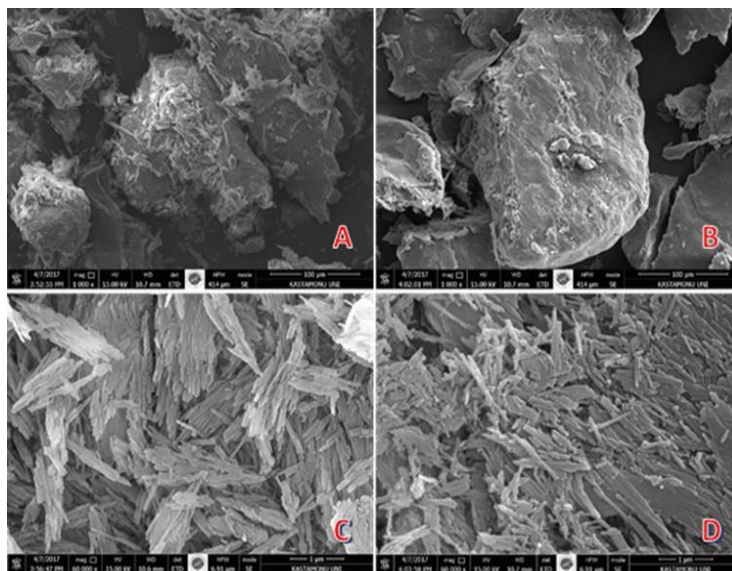
Figure 4. *SEM images of the antigorite-like-clay sample before (A, C) and after (B, D) adsorption of RB19.*

B, D). The rod structures changed from a scattered structure to regular forms and moved closer to each other with gaps between them identified to reduce (Figure 4: D). This situation shows that the antigorite-like clay sample adsorbed RB19 dye.

FT-IR Analysis. Figure 5 shows the infrared spectra for the serpentine clay, dye and serpentine clay after adsorption of dye. When the FTIR analysis of just the clay sample is investigated in general, the IR spectrum of the serpentine clay may be characterized in two groups. The first group was recorded in the interval from 3800-3500 cm⁻¹ with two IR bands observed at 3683 cm⁻¹ and 3642 cm⁻¹.
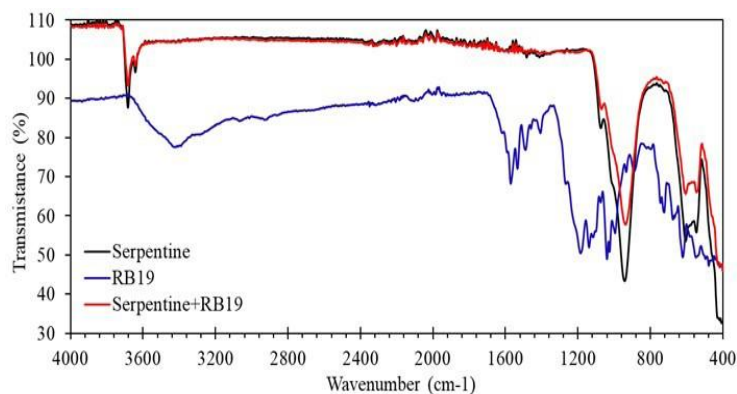
Figure 5. *FT-IR spectra of natural serpentine clay sample before and after adsorption of RB19.*

The IR band at 3683 cm⁻¹ can be assigned to the surface Mg-OH stretching vibration, whereas the second IR band at 3642 cm⁻¹ can be assigned to the inner Mg-OH stretching vibration (Kusiorowski et al., 2012; Lesci et al., 2014). The second group determined in the interval 1150-500 cm⁻¹ has IR bands at 1073, 1011, 940, 604 and 545 cm⁻¹. The band at 1073 cm⁻¹ can be assigned to the out-of-plane symmetric stretching vibration of the silica sheet, whereas the two IR bands at 1011 and 940 cm⁻¹ can be assigned to the in-plane Si-O stretching vibration (Bai et al., 2016; Crespo et al., 2019; Lacinska et al., 2016; Ristić et al., 2011). The peak point at 544 cm⁻¹ is due to Si-O bending vibration, while the peak point at 606 cm⁻¹ is due to Mg-OH bending vibration (Lu et al., 2019; Mellini et al., 2002). The FTIR spectrum of RB19 dye was observed to have N-H stretching vibration observed at 3417 cm⁻¹, –CH₂ groups seen at 2852

and 2926 cm⁻¹, and peaks for C-NH₂ stretching vibration at 1039 and 1182 cm⁻¹ (Yan et al., 2012; Zhang et al., 2015). The peaks for the vinyl sulfonyl group (-SO₂CH₂CH₂OSO₃Na) show a reduction in intensity after adsorption on serpentine.

Adsorption behaviors for RB19
Effect of pH. The solution pH has a significant effect on adsorption and ion exchange processes (Çoruh, 2008). The solution pH value is known to be one of the most important variables that can affect protonation of functional groups on the surface of the adsorbent (Ozdes et al., 2009). To determine the effect of the solution pH value on adsorption of RB19 by serpentine clay, initial RB19 concentration was set to 200 mg/L, temperature 25°C and adsorbent concentration 2 g/L while solution pH was changed from 3 to 9. The results obtained are given in Figure 6.
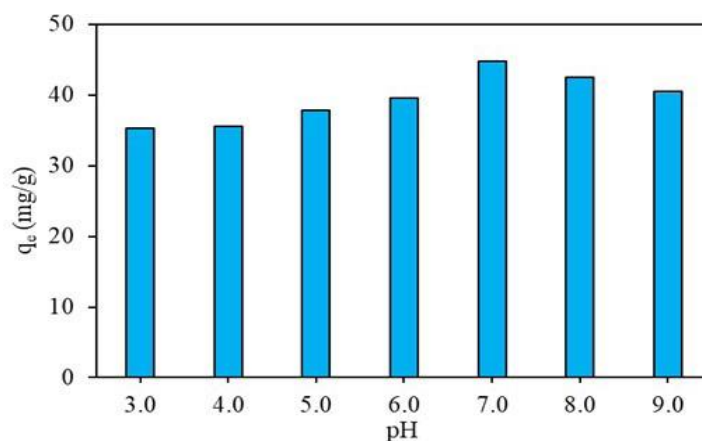
Figure 6. *Effect of the solution pH on the removal of RB19.*

The adsorption capacity was observed to rise from 35.3 mg/g to the highest value of 44.8 mg/g by increasing the solution pH value from 3 to 7. Increasing the solution pH from 7 to 9 reduced the adsorption capacity. Serpentine clay is reported to have positive surface load in a broad pH interval (up to 9.5) (Feng et al., 2013). The RB19 dye molecules have negative load due to anionic sulfonate- groups. As Mg^{2+} is the main cation on the octahedral layer in the serpentine clay, electrostatic attraction may form between the negative load sulfonate groups on the RB19 dye molecules. Additionally, the serpentine surface contains several amphoteric hydroxyl groups, so inner and outer sphere surface complexation may occur at the amphoteric edges during RB19 removal (Shaban et al., 2018). The reduction in RB19 removal in basic conditions may be linked to the intensity of negative loads in the adsorption system causing repulsion between the serpentine surface and RB19. With the presence of RB19 in solution, the increase in hydroxyl concentration reduces electrostatic attraction and

lowers adsorption capacity. The decrease in the amount of adsorption in acidic condition can be due to the ionization of the amine groups of the dye with H^+, which leads to positive charge on the molecules of the dye (Roushani et al., 2016). The repulsive electrostatic forces between the positive load on the surface of the adsorbent and the positive-load dye molecules increase and as a result adsorption reduces. As a result, pH 7 was determined to be the best solution pH.

Effect of adsorbent dosage. One of the parameters affecting adsorption is adsorbent dosage, determining the number of active sites on the adsorbent surface and as a result, this is important for general adsorption performance and commercial applications. With the aim of determining the effect of adsorbent dosage, initial RB19 concentration was set to 200 mg/L, pH to 7 and temperature to 25°C and adsorbent dosage was varied from 0.1-6 g/L. The experimental results are given in Figure 7.
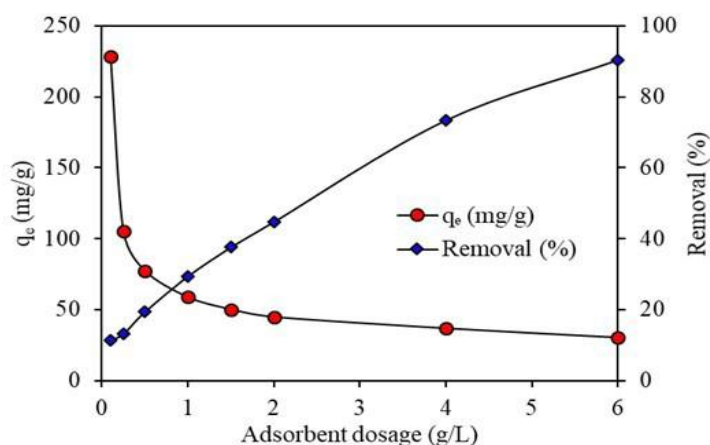
Figure 7. *Effect of adsorbent dosage on the removal of RB19.*

The results found that adsorption capacity of serpentine reduced from 228.6 mg/g to 30.1 mg/g linked to increased adsorbent dosage. This reduction in adsorption capacity may be explained by unsaturated contaminant sorption fields during the sorption process (Fil et al., 2014). Additionally, the RB19 removal efficiency increased from 11.4% to 90.4% with the increase in adsorbent amount. This increase in RB19 removal may be explained by the increase in surface area and pore volume.

Effect of initial concentration. With the aim of investigating initial RB19 concentration, experiments were performed with different initial RB19 concentrations from 10-200 mg/L and results are shown in Figure 8. Experiments were performed with initial pH 7, adsorbent dosage 2 g/L and temperature 25°C. With the increase in initial RB19 concentration, the dye removal efficiency reduced while the adsorption capacity increased. The RB19 removal efficiency decreased

from 95.5% to 44.8% with the increase in initial RB19 concentration. Due to the presence of empty binding sites on serpentine, RB19 removal efficiency is higher at low initial RB19 concentration. At high dye concentration, nearly all binding sites are filled, so removal efficiency reduced with initial RB19 concentration. The amount of RB19 adsorbed increased in stages with the increase in initial dye concentrations and the increase rate was

found to reduce at concentrations above 100 mg/L. Linked to initial RB19 concentration, adsorption capacities increased from 4.94 mg/g to 44.8 mg/g. The reason for this is the increase in concentration gradient at the solid/liquid contact interface due to the increase in external ion concentrations increasing driving forces with diffusion of RB19 on the serpentine surface (Tian et al., 2017).
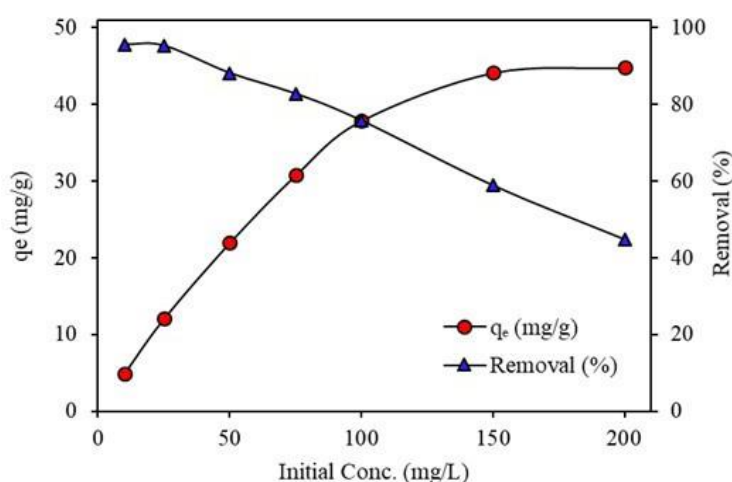
Figure 8. *Effect of initial RB19 concentration on the removal of RB19.*

Effect of temperature. Temperature is an important factor affecting the adsorption process. The variation in temperature directly affects the solubility of pollutant material in water and indirectly affects the degree of pollutant degradation (Wang et al., 2020). With the aim of determining the effect of

temperature on RB19 removal with serpentine, initial dye concentration was set to 50 mg/L, initial pH value to 7 and adsorbent dosage to 2 g/L, and temperature was investigated at 25, 35, 45 and 55°C. Figure 9 shows the results of experiments completed at different temperatures.
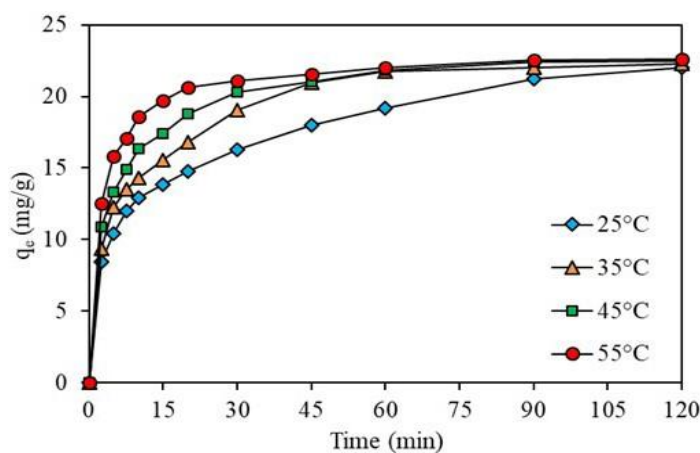
Figure 9. *Effect of temperature on adsorption of RB19 onto serpentine.*

Increasing the solution temperature from 20°C to 50°C was observed to have very little effect on the adsorption capacity at equilibrium and on removal of dye. However, stepped increase in temperature shortened the duration to reach adsorption equilibrium. Without reaching equilibrium, at t= 20 min, dye removal efficiency rose from 59.0% to 82.6% linked to the increase in temperature. There is a study with similar results in the literature (Ma et al., 2017).

Adsorption isotherm. The adsorption isotherm is used to identify the relationship between the adsorbate concentration within the adsorbent and solution when adsorption equilibrium is reached under certain experimental conditions (Zhang et al., 2018). In this study, the well-known Langmuir and Freundlich isotherms were used to assess equilibrium values obtained for RB19 adsorption. The Langmuir adsorption isotherm is an isotherm assuming active sites are homogeneously distributed on the adsorbent, the adsorption process is reversible and occurs in a single layer (Langmuir, 1918). The non-linear form of the Langmuir isotherm model is expressed in Eq. [6]:

$$q_e = \frac{q_m K_L C_e}{1 + K_L C_e} \qquad [6]$$

where q_m is the maximum adsorption capacity, C_e is equilibrium concentration of RB19, q_e is the equilibrium adsorption capacity of serpentine, and K_L is Langmuir constant. If experimental data are not sufficiently identified with the Langmuir

model, it is important to calculate the separation factor (R_L). The separation factor is defined in Eq. [7]:

$$q_e = \frac{q_m K_L C_e}{1 + K_L C_e} \qquad [7]$$

where R_L is a constant separation factor (dimensionless) of the solid-liquid adsorption system, K_L is the Langmuir equilibrium constant, and C_0 (mg/L) is the initial RB19 concentration. If the R_L value is between 0 and 1, it shows the adsorption process is favorable with the adsorbent used (Yasmin et al., 2019).

The Freundlich adsorption isotherm is used for equilibrium data with heterogeneous surface and adsorption features (Freundlich, 1907). The non-linear form of the Freundlich equation can be expressed as shown in Eq. [8]:

$$q_e = K_F C_e^n \qquad [8]$$

where K_F is the Freundlich constant, and *n* (dimensionless) is the Freundlich intensity parameter, which indicates the magnitude of the adsorption driving force or the surface heterogeneity. According to the Freundlich theory, the adsorption isotherm becomes linear when n=1, favorable when n<1, and unfavorable when n>1. Isotherm constants were analyzed using the nonlinear trial and error method with the solver add-in to Microsoft Office Excel. The correlation coefficient (R^2) and root mean square error (RMSE) were calculated to assess the fit of the models. Table 4 gives the constants, R^2 and RMSE calculated for the isotherm models.

Table 4. *Isotherm constants for adsorption of RB19 onto serpentine.*

Isotherm model	Parameters	Values
Langmuir	q_m (mg/g)	47.01
	K_L (L/mg)	0.1703
	R^2	0.9822
	RMSE	1.8069
Freundlich	K_F [(mg/g)/(mg/L)^n]	13.49
	n	0.2768
	R^2	0.9288
	RMSE	3.6130

According to isotherm results, the Langmuir model has higher R^2 and lower RMSE values compared to the Freundlich model, and appears more suitable to explain the adsorption of RB19 on serpentine. As a result, it can be said that adsorption occurs on a homogeneous surface rather than a heterogeneous surface and the immobilized RB19 ions form a monolayer on the positively-charged binding sites of the serpentine (Zayed et al., 2018). The R_L values

calculated with the aid of Equation [7] vary from 0.37-0.03. This shows that adsorption of RB19 on serpentine is favorable. The maximum adsorption capacity (q_m) calculated for adsorption of RB19 on serpentine with the Langmuir isotherm model was found to be 47.01 mg/g. Additionally, the comparison with adsorption capacity for removal of different pollutants using serpentine clay is given in Table 5.

Table 5. *Comparison of adsorption capacity in the removal of different pollutants.*

Adsorbed	Adsorbent	q_{max} (mg/g)	$q_{max, exp}$ (mg/g)	pH	References
Cadmium	Thermal activated serpentine	17.68	15.21	8.12	(Cao et al. 2017)
Congo red	Thermal and acidic treatment	93.45	15.36	3.0	(Shaban et al. 2018)
Methylene blue	Thermal and acidic treatment	58.48	38.46	8.0	(Shaban et al. 2018)
Cr(VI)	Thermal and acidic treatment	76.33	37.87	3.0	(Shaban et al. 2018)
Pb(II)	Thermal activation modification	131.4	67.19	8.44	(Cao et al. 2019)
RB19	Natural serpentine	44.8	47.01	7.0	Present study

Adsorption kinetics. The adsorption rate for RB19 dye on serpentine clay used the pseudo-first-order (PFO) kinetic model (Eq. [9]) (Lagergren, 1898) and pseudo-second-order (PSO) kinetic model (Eq. [10]) (Blanchard et al., 1984) to identify the adsorption capacity under equilibrium and non-equilibrium conditions:

$$q_t = q_e\left(1 - e^{-k_1 t}\right) \qquad [9]$$

$$q_t = \frac{k_2 q_e^2 t}{1 + k_2 q_e t} \qquad [10]$$

where, k_1 is the rate constant for the PFO kinetic model (1/min); k_2 is the rate constant for the PSO kinetic model (g/mg/min); q_t and q_e represent the RB19 adsorption capacity at time t and equilibrium (mg/g), respectively.

It was stated that using the linear forms of these kinetic models causes erroneous results and as a result, mistaken decisions. Additionally, the literature states that better results are obtained for fit to experimental data when non-linear forms are used compared to linear forms (Lima et al., 2015; Lin and Wang, 2009; Simonin, 2016). As a result, the maximum adsorption capacity (at equilibrium) and rate constant values were obtained using the non-linear method. Table 6 shows the kinetic parameters and determination coefficients obtained for the PFO and PSO model at different temperatures. When the determination coefficients are investigated, the PSO model explains the adsorption process of RB19 on serpentine better. Additionally, the adsorption capacity values calculated with the PSO model are observed to be closer and more consistent with the measured adsorption capacity compared to the PFO model.

Table 6. *Kinetics parameters obtained from pseudo-first-order model and pseudo-second-order model for the removal of RB19 by serpentine at different temperatures.*

Temperature (°C)	$q_{e, exp}$ (mg/g)	Pseudo-first-order			Pseudo-second-order		
		k_1	$q_{e, cal}$	R^2	k_2	$q_{e, cal}$	R^2
25	21.96	0.1224	18.98	0.8877	0.0078	21.21	0.9585
35	22.25	0.1391	20.60	0.9227	0.0089	22.67	0.9785
45	22.46	0.1852	20.88	0.9437	0.0124	22.70	0.9903
55	22.60	0.2693	21.32	0.9700	0.0198	22.79	0.9986

Conclusions

Within the scope of this study, unprocessed clay (serpentine) was used to remove anionic dye. The serpentine group clay sample was characterized in detail with a variety of analytic techniques like XRD, FTIR, SEM, TGA, XRF and BET. Structural research using XRD techniques revealed the presence of antigorite and chrysotile clay minerals as crystal phases within the serpentine composition. The results obtained from adsorption experiments found the adsorption of RB19 dye on serpentine was explained better by the Langmuir isotherm model compared to the Freundlich isotherm model. Serpentine was observed to have maximum RB19 adsorption capacity of 44.8 mg/g. Two different kinetic models were applied to experimental data. The kinetic results showed that the adsorption of the RB19 by the serpentine conforms to the PSO kinetic model. Additionally, temperature did not have much effect on the equilibrium adsorption capacity; however, it increased removal rates. The use of serpentine clay to remove RB19 from wastewater was concluded to be a low cost and effective adsorbent choice.

Acknowledgements

Conflicts of interest

On behalf of all authors, the corresponding author states that there is no conflict of interest.

References

ARSHAD R., BOKHARI T.H., KHOSA K.K., BHATTI I.A., MUNIR M., IQBAL M., IQBAL D.N., KHAN M.I., IQBAL M., NAZIR A. (2020) Gamma radiation induced degradation of anthraquinone Reactive Blue-19 dye using hydrogen peroxide as oxidizing agent. Radiation Physics and Chemistry, 168:108637. https://doi.org/10.1016/j.radphyschem.2019.108637

BAI Z.M., YANG N., GUO M., LI S. (2016) Antigorite: Mineralogical characterization and friction performances. Tribology International, 101:115–121. https://doi.org/10.1016/j.triboint.2016.03.036

BALLOTIN F.C., NASCIMENTO M., VIEIRA S.S., BERTOLI A.C., CARMIGNANO O., DE CARVALHO TEIXEIRA A.P., LAGO R.M. (2020) Natural Mg silicates with different structures and morphologies: Reaction with K to produce K_2MgSiO_4 catalyst for biodiesel production. International Journal of Minerals, Metallurgy and Materials, 27:46–54. https://doi.org/10.1007/s12613-019-1891-9

BILAL M., RASHEED T., IQBAL H.M.N., LI C., WANG H., HU, H., WANG W., ZHANG X. (2018) Photocatalytic degradation, toxicological assessment and degradation pathway of C.I. Reactive Blue 19 dye. Chemical Engineering Research and Design, 129:384–390. https://doi.org/10.1016/j.cherd.2017.11.040

BLANCHARD G., MAUNAYE M., MARTIN G. (1984) Removal of heavy metals from waters by means of natural zeolites. Water Research, 18(12):1501–1507. https://doi.org/10.1016/0043-1354(84)90124-6

CAO C.Y., LIANG C.H., YIN Y., DU L.Y. (2017) Thermal activation of serpentine for adsorption of cadmium. Journal of Hazardous Materials, 329:222–229. https://doi.org/10.1016/j.jhazmat.2017.01.042

CAO C.Y., YU B., WANG M., ZHAO Y.Y., ZHAO Y.H. (2019) Adsorption properties of Pb^{2+} on thermal-activated

serpentine. Separation Science and Technology, 54(18):3037-3045. https://doi.org/10.1080/01496395.2019.1565776

CHAUDHARI A.U., PAUL D., DHOTRE D., KODAM K.M. (2017) Effective biotransformation and detoxification of anthraquinone dye reactive blue 4 by using aerobic bacterial granules. Water Research, 122:603–613. https://doi.org/10.1016/j.watres.2017.06.005

CHENG T.W., DING Y.C., CHIU J.P. (2002) A study of synthetic forsterite refractory materials using waste serpentine cutting. Minerals Engineering, 15(4):271–275. https://doi.org/10.1016/S0892-6875(02)00021-3

CHINOUNE K., BENTALEB K., BOUBERKA Z., NADIM A., MASCHKE U. (2016) Adsorption of reactive dyes from aqueous solution by dirty bentonite. Applied Clay Science, 123:64–75. https://doi.org/10.1016/j.clay.2016.01.006

CORUH S. (2008) The removal of zinc ions by natural and conditioned clinoptilolites. Desalination, 225(1-3):41–57. https://doi.org/10.1016/j.desal.2007.06.015

CRESPO M.A.R., GOMEZ D.P., GARCIA M.V.V., AMORES J.M.G., ESCRIBANO V.S. (2019) Characterization of serpentines from different regions by transmission electron microscopy, X-ray diffraction, BET specific surface area and vibrational and electronic spectroscopy. Fibers, 7(5):47. https://doi.org/10.3390/fib7050047

DEGERMENCI G.D., DEGERMENCI N., AYVAOGLU V., DURMAZ E., CAKIR D., AKAN E. (2019) Adsorption of reactive dyes on lignocellulosic waste; characterization, equilibrium, kinetic and thermodynamic studies. Journal of Cleaner Production, 225:1220–1229. https://doi.org/10.1016/j.jclepro.2019.03.260

DEGERMENCI N., AKYOL K. (2020) Decolorization of the Reactive Blue 19 from Aqueous Solutions with the Fenton Oxidation Process and Modeling with Deep Neural Networks. Water Air & Soil Pollution, 231:72. https://doi.org/10.1007/s11270-020-4402-8

DLUGOGORSKI B.Z., BALUCAN R.D. (2014) Dehydroxylation of serpentine minerals: Implications for mineral carbonation. Renewable and Sustainable Energy Reviews, 31:353–367. https://doi.org/10.1016/j.rser.2013.11.002

EMRULLAHOGLU ABI C.B., GUREL S.B., KILINC D., EMRULLAHOGLU F. (2015) Production of forsterite from serpentine - Effects of magnesium chloride hexahydrate addition. Advanced Powder Technology, 26(3):947–953. https://doi.org/10.1016/j.apt.2015.03.011

FENG B., LU Y.P., FENG Q.M., DING P., LUO N. (2013) Mechanisms of surface charge development of serpentine mineral. Transactions of Nonferrous Metals Society of China, 23(4):1123–1128. https://doi.org/10.1016/S1003-6326(13)62574-1

FIL B.A., YILMAZ M.T., BAYAR S., ELKOCA M.T. (2014) Investigation of adsorption of the dyestuff astrazon red violet 3rn (basic violet 16) on montmorillonite clay. Brazilian Journal of Chemical Engineering, 31(1):171–182. https://doi.org/10.1590/S0104-66322014000100016

FREUNDLICH H. (1907) Über die Adsorption in Lösungen. Zeitschrift für Physikalische Chemie, 57(1):385–470. https://doi.org/10.1515/zpch-1907-5723

GURTEKIN G., ALBAYRAK M. (2006) Thermal Reaction of Antigotire: A XRD, DTA-TG Work. Bulletin of the Mineral Research and Exploration, 133(133):41–49.

HE C.-C., HU C.-Y., LO S.-L. (2016) Evaluation of sono-electrocoagulation for the removal of Reactive Blue 19 passive film removed by ultrasound. Separation and Purification Technology, 165:107–113. https://doi.org/10.1016/j.seppur.2016.03.047

HOREN H., SOUBRAND M., KIRCZAK J., JOUSSEIN E., NEEL C. (2014) Magnetic characterization of ferrichromite in soils developed on serpentinites under temperate climate. Geoderma, 235–236:83–89. https://doi.org/10.1016/j.geoderma.2014.06.026

HRSAK D., SUCIK G., LAZIC L. 2008. The thermophysical properties of serpentinite. Metalurgija, 47:29–31.

HUANG P., LI Z., CHEN M., HU H., LEI Z., ZHANG Q., YUAN W. (2017) Mechanochemical activation of serpentine for recovering Cu(II) from wastewater. Applied Clay Science, 149:1–7. https://doi.org/10.1016/j.clay.2017.08.030

ISAH U.A., ABDULRAHEEM G., BALA S., MUHAMMAD S., ABDULLAHI M. (2015) Kinetics, equilibrium and thermodynamics studies of C.I. Reactive Blue 19 dye adsorption on coconut shell based activated carbon. International Biodeterioration & Biodegradation, 102:265–273. https://doi.org/10.1016/j.ibiod.2015.04.006

KARUNARATNE P.C.T., ROHAN FERNANDO G.R. (2015) Non-Asbestos form building materials for Sustainable City Planning in Sri Lanka. In: International Conference on Cities, Peoples and Places; 26-27 October 2015; Sri Lanka. p. 1-13.

KHAN M.A.N., SIDDIQUE M., WAHID F., KHAN R. (2015) Removal of reactive blue 19 dye by sono, photo and sonophotocatalytic oxidation using visible light. Ultrasonics Sonochemistry, 26:370–377. https://doi.org/10.1016/j.ultsonch.2015.04.012

KOCAMAN S. (2020) Removal of methylene blue dye from aqueous solutions by adsorption on levulinic acid-modified natural shells. International Journal of Phytoremediation, 22:885–895. https://doi.org/10.1080/15226514.2020.1736512

KUSIOROWSKI R., ZAREMBAT., PIOTROWSKI J., ADAMEK J. (2012) Thermal decomposition of different types of asbestos. Journal of Thermal Analysis and Calorimetry, 109:693–704. https://doi.org/10.1007/s10973-012-2222-9

LACINSKA A.M., STYLES M.T., BATEMAN K., WAGNER D., HALL M.R., GOWING C., BROWN P.D. (2016) Acid-dissolution of antigorite, chrysotile and lizardite for ex situ carbon capture and storage by mineralisation. Chemical Geology, 437:153–169. https://doi.org/10.1016/j.chemgeo.2016.05.015

LAGERGREN S. (1898) About the theory of so-called adsorption of soluble substances. Kungliga Svenska Vetenskapsakademiens Handlingar, 24:1–39.

LANGMUIR I., (1918) The adsorption of gases on plane surfaces of glass, mica and platinum. Journal of the American Chemical Society, 40(9):1361–1403. https://doi.org/10.1021/ja02242a004

LESCI I.G., BALDUCCI G., PIERINI F., SOAVI F., ROVERI N. (2014) Surface features and thermal stability of mesoporous Fe doped geoinspired synthetic chrysotile nanotubes. Microporous and Mesoporous Materials, 197:8–16. https://doi.org/10.1016/j.micromeso.2014.06.002

LIMA E.C., ADEBAYO M.A., MACHADO F.M., (2015) Kinetic and equilibrium models of adsorption. In: Bergmann C.P., Machado F.M. (Eds.), Carbon Nanostructures. Springer International Publishing, pp.33–69. https://doi.org/10.1007/978-3-319-18875-1_3

LIN J., WANG L. (2009) Comparison between linear and non-linear forms of pseudo-first-order and pseudo-second-order adsorption kinetic models for the removal of methylene blue by activated carbon. Frontiers of Environmental Science & Engineering in China, 3:320–324. https://doi.org/10.1007/s11783-009-0030-7

LU J., SUN M., YUAN Z., QI S., TONG Z., LI L., MENG Q. (2019) Innovative insight for sodium hexametaphosphate interaction with serpentine. Colloids and Surfaces A: Physicochemical and Engineering Aspects, 560:35–41. https://doi.org/10.1016/j.colsurfa.2018.09.076

MA D., ZHU B., CAO B., WANG J., ZHANG J. (2017) Fabrication of the novel hydrogel based on waste corn stalk for removal of methylene blue dye from aqueous solution. Applied Surface Science, 422:944–952. https://doi.org/10.1016/j.apsusc.2017.06.072

MAROTO-VALER M.M., FAUTH D.J., KUCHTA M.E., ZHANG Y., ANDRESEN J.M. (2005) Activation of magnesium rich minerals as carbonation feedstock materials for CO_2 sequestration. Fuel Processing Technology, 86(14-15):1627–1645. https://doi.org/10.1016/j.fuproc.2005.01.017

MELLINI M., FUCHS Y., VITI C., LEMAIRE C., LINARES J. (2002) Insights into the antigorite structure from Mossbauer and FTIR spectroscopies. European Journal of Mineralogy, 14(1):97–104. https://doi.org/10.1127/0935-1221/2002/0014-0097

MELO R.P.F., BARROS NETO E.L., NUNES S.K.S., CASTRO DANTAS T.N., DANTAS NETO A.A. (2018) Removal of Reactive Blue 14 dye using micellar solubilization followed by ionic flocculation of surfactants. Separation and Purification Technology, 191:161–166. https://doi.org/10.1016/j.seppur.2017.09.029

MOMCILOVIC M.Z., RANDELOVIC M.S., PURENOVIC M.M., DORDEVIC J.S., ONJIA A., MATOVIC B. (2016) Morpho-structural, adsorption and electrochemical characteristics of serpentinite. Separation and Purification Technology, 163:72–78. https://doi.org/10.1016/j.seppur.2016.02.042

NGA N.K., THUY CHAU N.T., VIET P.H. (2020) Preparationandcharacterizationofachitosan/MgOcomposite for the effective removal of reactive blue 19 dye from aqueous solution. Journal of Science: Advanced Materials and Devices, 5(1):65–72. https://doi.org/10.1016/j.jsamd.2020.01.009

NIDHEESH P.V., ZHOU M., OTURAN M.A. (2018) An overview on the removal of synthetic dyes from water by electrochemical advanced oxidation processes. Chemosphere, 197, 210–227. https://doi.org/10.1016/j.chemosphere.2017.12.195

OZDES D., GUNDOGDU A., KEMER B., DURAN C., SENTURK H.B., SOYLAK M. (2009) Removal of Pb(II) ions from aqueous solution by a waste mud from copper mine industry: Equilibrium, kinetic and thermodynamic study. Journal of Hazardous Materials, 166(2-3):1480–1487. https://doi.org/10.1016/j.jhazmat.2008.12.073

PATTERSON A.L. (1939) The scherrer formula for X-ray particle size determination. Physical Review, 56(10):978–982. https://doi.org/10.1103/PhysRev.56.978

RISTIC M., CZAKO-NAGY I., MUSIC S., VERTES A. (2011) Spectroscopic characterization of chrysotile asbestos from different regions. Journal of Molecular Structure, 993(1-3):120–126. https://doi.org/10.1016/j.molstruc.2010.10.005

ROUSHANI M., SAEDI Z., MUSA BEYGI T. (2016) Anionic dyes removal from aqueous solution using TMU-16 and TMU-16-NH2 as isoreticular nanoporous metal organic frameworks. Journal of the Taiwan Institute of Chemical Engineers, 66:164–171. https://doi.org/10.1016/j.jtice.2016.06.012

SHABAN M., ABUKHADRA M.R., KHAN A.A.P., JIBALI B.M. (2018) Removal of Congo red, methylene blue and Cr(VI) ions from water using natural serpentine. Journal of the Taiwan Institute of Chemical Engineers, 82:102–116. https://doi.org/10.1016/j.jtice.2017.10.023

SIMONIN J.P. (2016) On the comparison of pseudo-first order and pseudo-second order rate laws in the modeling of adsorption kinetics. Chemical Engineering Journal, 300:254–263. https://doi.org/10.1016/j.cej.2016.04.079

TAHERI M., MOGHADDAM M.R.A., ARAMI M. (2013) Techno-economical optimization of Reactive Blue 19 removal by combined electrocoagulation/coagulation process through MOPSO using RSM and ANFIS models. Journal of Environmental Management, 128:798–806. https://doi.org/10.1016/j.jenvman.2013.06.029

TEIR S., REVITZER H., ELONEVA S., FOGELHOLM C.J., ZEVENHOVEN R. (2007) Dissolution of natural serpentinite in mineral and organic acids. International Journal of Mineral Processing, 83(1-2):36–46. https://doi.org/10.1016/j.minpro.2007.04.001

THOMMES M., KANEKO K., NEIMARK A.V., OLIVIER J.P., RODRIGUEZ-REINOSO F., ROUQUEROL J., SING, K.S.W. (2015) Physisorption of gases, with special reference to the evaluation of surface area and pore size distribution (IUPAC Technical Report). Pure and Applied Chemistry, 87(9-10):1051–1069. https://doi.org/10.1515/pac-2014-1117

TIAN G., WANG W., ZONG L., WANG A. (2017) MgO/palygorskite adsorbent derived from natural Mg-rich brine and palygorskite for high-efficient removal of Cd(II) and Zn(II) ions. Journal of Environmental Chemical Engineering, 5(1):1027–1036. https://doi.org/10.1016/j.jece.2017.01.028

TKACZYK A., MITROWSKA K., POSYNIAK A. (2020) Synthetic organic dyes as contaminants of the aquatic environment and their implications for ecosystems: A review. Science of The Total Environment, 717:137222. https://doi.org/10.1016/j.scitotenv.2020.137222

VASCONCELOS V.M., MIGLIORINI F.L., STETER J.R., BALDAN M.R., FERREIRA N.G., DE VASCONCELOS LANZA M.R. (2016) Electrochemical oxidation of RB-19 dye using a highly BDD/Ti: Proposed pathway and toxicity. Journal of Environmental Chemical Engineering, 4(4A):3900–3909. https://doi.org/10.1016/j.jece.2016.08.029

VITI C. (2010) Serpentine minerals discrimination by thermal analysis. American Mineralogist, 95(4):631–638. https://doi.org/10.2138/am.2010.3366

VITI C., GIACOBBE C., GUALTIERI A.F. (2011) Quantitative determination of chrysotile in massive serpentinites using DTA: Implications for asbestos determinations. American Mineralogist, 96(7):1003–1011. https://doi.org/10.2138/am.2011.3734

WANG J., QIN L., LIN J., ZHU J., ZHANG Y., LIU J., VAN DER BRUGGEN B. (2017) Enzymatic construction of antibacterial ultrathin membranes for dyes removal. Chemical Engineering Journal, 323:56–63. https://doi.org/10.1016/j.cej.2017.04.089

WANG X., CHEN A., CHEN B., WANG L. (2020) Adsorption of phenol and bisphenol A on river sediments: Effects of particle size, humic acid, pH and temperature. Ecotoxicology and Environmental Safety, 204:111093. https://doi.org/10.1016/j.ecoenv.2020.111093

YALCIN H., BOZKAYA O. (2006) Mineralogy and geochemistry of Paleocene ultramafic- and sedimentary-hosted talc deposits in the southern part of the Sivas Basin, Turkey. Clays and Clay Minerals, 54:333–350. https://doi.org/10.1346/ccmn.2006.0540305

YAN W., LIU D., TAN D., YUAN P., CHEN M. (2012) FTIR spectroscopy study of the structure changes of palygorskite under heating. Spectrochimica Acta Part A: Molecular and Biomolecular Spectroscopy, 97:1052–1057. https://doi.org/10.1016/j.saa.2012.07.085

YASMIN R., AFTAB K., KASHIF M. (2019) Removal of microcystin-LR from aqueous solution using Moringa oleifera Lam. seeds. Water Science and Technology, 79(1):104–113. https://doi.org/10.2166/wst.2019.006

ZAYED A.M., ABDEL WAHED M.S.M., MOHAMED E.A., SILLANPAA M. (2018) Insights on the role of organic matters of some Egyptian clays in methyl orange adsorption: Isotherm and kinetic studies. Applied Clay Science, 166:49–60. https://doi.org/10.1016/ j.clay.2018.09.013

ZHANG K., LI H., XU X., YU H. (2018) Synthesis of reduced graphene oxide/NiO nanocomposites for the removal of Cr(VI) from aqueous water by adsorption. Microporous and Mesoporous Materials, 255:7–14. https:// doi.org/10.1016/j.micromeso.2017.07.037

ZHANG Y., WANG W., ZHANG J., LIU P., WANG A. (2015) A comparative study about adsorption of natural palygorskite for methylene blue. Chemical Engineering Journal, 262:390–398. https://doi.org/10.1016/j. cej.2014.10.009